

Modification of ground-state chemical reactivity via light–matter coherence in infrared cavities

Wonmi Ahn¹, Johan F. Triana², Felipe Recabal², Felipe Herrera^{2,3*}, Blake S. Simpkins^{4*}

Reaction-rate modifications for chemical processes due to strong coupling between reactant molecular vibrations and the cavity vacuum have been reported; however, no currently accepted mechanisms explain these observations. In this work, reaction-rate constants were extracted from evolving cavity transmission spectra, revealing resonant suppression of the intracavity reaction rate for alcoholysis of phenyl isocyanate with cyclohexanol. We observed up to an 80% suppression of the rate by tuning cavity modes to be resonant with the reactant isocyanate (NCO) stretch, the product carbonyl (CO) stretch, and cooperative reactant–solvent modes (CH). These results were interpreted using an open quantum system model that predicted resonant modifications of the vibrational distribution of reactants from canonical statistics as a result of light–matter quantum coherences, suggesting links to explore between chemistry and quantum science.

Controlling chemical reactions with electromagnetic fields is a long-standing goal in chemistry and physics (1, 2). Femtosecond laser pulses can transiently excite vibrational modes of reactant molecules to selectively promote breaking or forming of chemical bonds (3–5). However, fast energy redistribution in polyatomic molecules severely limits this approach, despite efforts to overcome this obstacle using laser pulse shaping (6, 7).

Chemical control without lasers has been recently demonstrated using cavities (8–12). In this approach, hybrid light–matter polariton states arise from strong interactions of dipole-allowed molecular transitions with the cavity vacuum at optical (13) and infrared frequencies (14–16). Experiments show inhibition of excited-state processes such as photoisomerization (17) and photobleaching (18) in visible cavities and also modification of bond formation and cleavage rates in infrared cavities as a result of vibrational strong coupling (VSC) (8–10, 19). VSC is characterized by collective molecular response in transmission (20, 21), a spatial dependence of the interaction that follows the mode profile (22, 23), and reversible modulation of the system using ultrafast lasers (24, 25) or electrochemistry (26, 27).

Achieving coupling-induced selective chemistry would enable chemical catalysis by design, but challenges to its reproducibility (28, 29) and lack of mechanistic explanation have stilled progress. Here, we report robust experimental evidence of cavity-modified chemistry and describe a theory consistent with measurements.

We studied the alcoholysis of phenyl isocyanate (PHI) with cyclohexanol (CHol) in tetrahydrofuran (THF) to give urethane [cyclohexyl carbamate (CC)]. The reaction is exothermal (30), has a low activation energy (31), and resonant cavity modes can be tuned to reactant, product, or solvent vibrational modes. We measured a strong cavity-tuning dependence of the reaction kinetics, with rate constants reduced by 30 to 80%, and developed a quantum model that qualitatively agrees with observations and provides mechanistic understanding for intracavity reaction kinetics. Our theory proposes that the intracavity reactivity depends on stationary light–matter coherences, and we discuss the importance of energy disorder in preserving coherence over chemical time scales.

Results and discussion

The alcoholysis of isocyanates is well understood (31–33) and proceeds through concerted nucleophilic addition at the NC bond in isocyanate (31, 33, 34). The geometry of the PHI-CHol complex (Fig. 1A) involves an NHO hydrogen bond that evolves into a cyclic NHOC structure in the transition state (3). Cleavage of the HO bond results in ring opening and exothermic formation of urethane ($\Delta H_{\text{rxn}} \approx -20.5$ kcal/mol) with activation energy of 6.7 kcal/mol (2343 cm^{-1}) in THF. The second-order rate constant at room temperature is $k_0 = 0.59 \times 10^{-5} \text{ M}^{-1}\text{s}^{-1}$ (3). Back reactions are negligible.

We injected the reactant solution into a thin-layer cell bounded by transparent CaF_2 windows, for out-of-cavity control measurements, or by Au-coated CaF_2 windows, for cavity-coupled measurements [Fig. 1B; additional details in section 1 of the supplementary materials (SM)]. Figure 1C shows two sets of transmission spectra. For control measurements (upper curves, red), reactant bands decreased (NCO stretch of PHI at $\sim 2260 \text{ cm}^{-1}$ and OH band of CHol at $\sim 3470 \text{ cm}^{-1}$), and

product bands grew (CO at 1730 cm^{-1} and at 3293 cm^{-1} ; see detailed spectra in figs. S1–S2). The NCO band absorption was converted to reactant concentration through direct proportionality (see procedure in section 1 of the SM and fig. S3 for extinction coefficient calibration), then inverted and plotted against time (Fig. 1D), yielding a line whose slope equaled the second-order rate constant (35). The average of six such measurements gave a control rate constant $k_0 = (2.34 \pm 0.2) \times 10^{-5} \text{ M}^{-1}\text{s}^{-1}$ (datasets in fig. S4). This rate was higher than in previous reports (32), which involved lower reactant concentrations. The rates measured under our conditions were consistent in independent measurements performed in a period of 24 months, with all reactions (control and cavity-coupled) carried out using the same initial reactant concentrations.

Typical transmission spectra for a cavity-coupled sample are shown in Fig. 1C (lower curves, blue). These example data exhibited multiple resonant peaks, with one coupled to the NCO band of PHI (2260 cm^{-1}), giving a splitting at normal incidence of 112 cm^{-1} (cavity $Q \sim 100$, cavity linewidth $\kappa \approx 38 \text{ cm}^{-1}$; see table S2). These evolving transmission spectra were fit to a function that accounted for the absorbance of the intracavity medium (Fig. 1E), which, again, was directly proportional to reactant concentration. We inverted and plotted this data (Fig. 1F) to extract a rate constant $k = (1.48 \pm 0.2) \times 10^{-5} \text{ M}^{-1}\text{s}^{-1}$ for this sample, $\sim 37\%$ lower than uncoupled controls. Collection of the entire cavity dispersion allowed identification and fitting of spectra showing strong interaction with the mode of interest regardless of tuning at normal incidence [see the model in section 3.3 of the SM and (14, 21, 23, 25, 27)].

Reaction rates were extracted for different cavities. The resulting “action spectrum” (9) is shown in Fig. 2A. The initial (blue) and final (orange) transmission spectra of the control solution are shown to identify relevant vibrational modes. There was a strong dependence of the reaction rate on the cavity mode tuning, with rate suppression due to VSC on reactant (NCO), product (CO), and cooperative reactant–solvent (CH) modes (full dataset in fig. S8 and table S1). Cavity-induced suppression spanned 30 to 80%, relative to uncoupled controls. The largest suppression was found for cavities tuned to the NCO reactant mode, with a frequency dependence that closely followed the shape of the NCO absorption band. The rate constants for far-detuned cavities (squares) were close to the out-of-cavity rates ($k/k_0 \sim 0.91$; see table S1). Figure 2B shows representative inverse concentration plots and linear fits for cavities tuned to the reactant NCO and reactant–solvent CH bands, highlighting the lower slopes (rates), relative to out-of-cavity controls. Our mechanistic discussion below

¹UNAM — National Nanotechnology Research Center and Institute of Materials Science and Nanotechnology, Bilkent University, Ankara, Turkey. ²Department of Physics, Universidad de Santiago de Chile, Santiago, Chile. ³Millennium Institute for Research in Optics (MIRO), Concepción, Chile. ⁴Chemistry Division, US Naval Research Laboratory, Washington, DC, USA. *Corresponding author. Email: blake.simpkins@nrl.navy.mil (B.S.S.); felipe.herrera@usach.cl (F.H.)



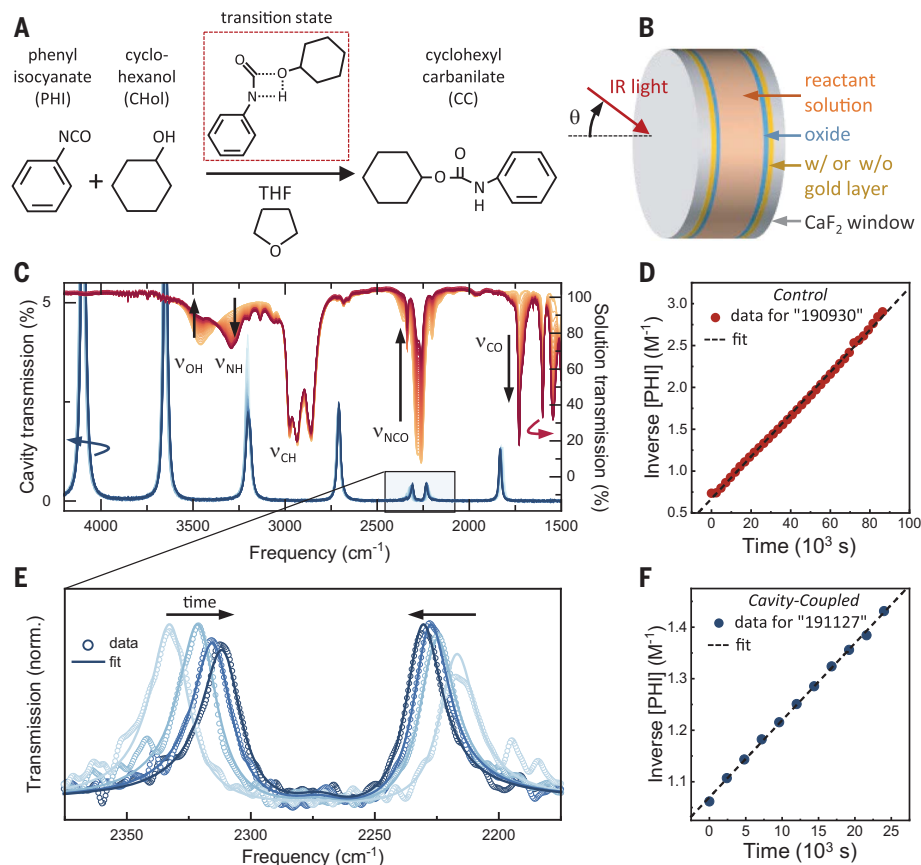


Fig. 1. Description of urethane monomer formation and reaction monitoring. (A) The reactants phenyl isocyanate (PHI) and cyclohexanol (CHol) were combined in tetrahydrofuran (THF) to form cyclohexyl carbanilate (CC). (B) Solution was contained between two CaF_2 windows that were either transparent (for control measurements) or coated with Au/SiO_2 (for cavity-coupled experiments). (C) Time-dependent Fourier transform infrared transmission spectra for out-of-cavity control measurements (red hues) showed reactant absorptions, ν_{NCO} of PHI at 2260 cm^{-1} and ν_{OH} of CHol at 3470 cm^{-1} , diminished as the reaction proceeded, while product features, ν_{CO} at 1730 cm^{-1} and ν_{NH} at 3293 cm^{-1} , increased. The ν_{NCO} absorption was converted to PHI concentration, inverted, and plotted versus time to extract the second-order reaction rate constant as shown in (D). The blue curves in (C) correspond to a time series of cavity-coupled transmission spectra showing strong coupling between the cavity and NCO vibrational mode of the PHI reactant. These spectra were fit, as shown in (E), to yield time-dependent PHI concentration, which was inverted, plotted, and fit to yield the reaction rate constant under cavity-coupled conditions. One typical cavity-coupled dataset is shown in (F).

focuses on the NCO band because it plays a prominent role in the reaction, however, modification of one mode can influence others (intramolecular vibrational relaxation, Fermi coupling, etc.). Further, we note that the product-coupled cavity also supported a higher-order mode that weakly coupled to the reactant OH mode ($\sim 3500\text{ cm}^{-1}$), however, we have only highlighted modes under strong coupling. The role of weak coupling in chemical reactivity has yet to be fully understood.

Our mechanistic description of VSC-modified reactivity started by modeling the vibrational structure of the PHI molecule in the frequency region of the NCO band, which includes a fundamental NCO stretch, ν_6 , and a Fermi resonance between ν_6 and a combination of

low-frequency CH bending modes (analysis in section 4 of the SM). The NCO fundamental at 2260 cm^{-1} was inhomogeneously broadened (full width at half maximum $\approx 47\text{ cm}^{-1}$; see fig. S13). We modeled an ensemble of N reactant NCO vibrations under VSC at 300 K, considering vibrational relaxation, cavity decay, thermalization, and many-body correlations, using an open quantum system approach (see sections 5 and 6 of the SM). Field-dependent dipole self-energy terms (36) were not included. The theory suggested that although the coupled vibration-cavity system was at thermal equilibrium with its environment, as confirmed by experiments (37), when tracing out the photonic degrees of freedom, the stationary vibrational population of reactants could deviate

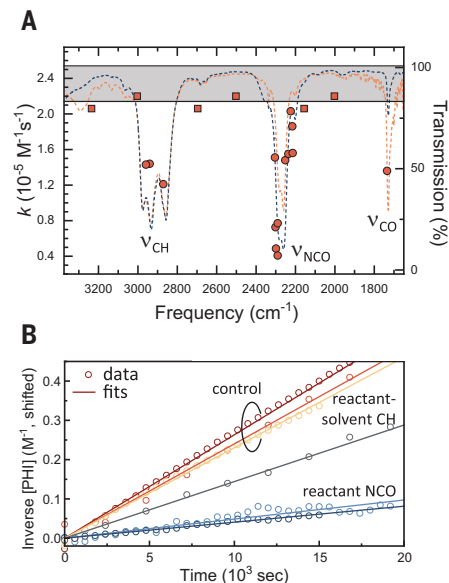


Fig. 2. Cavity-modified chemical reactivity.

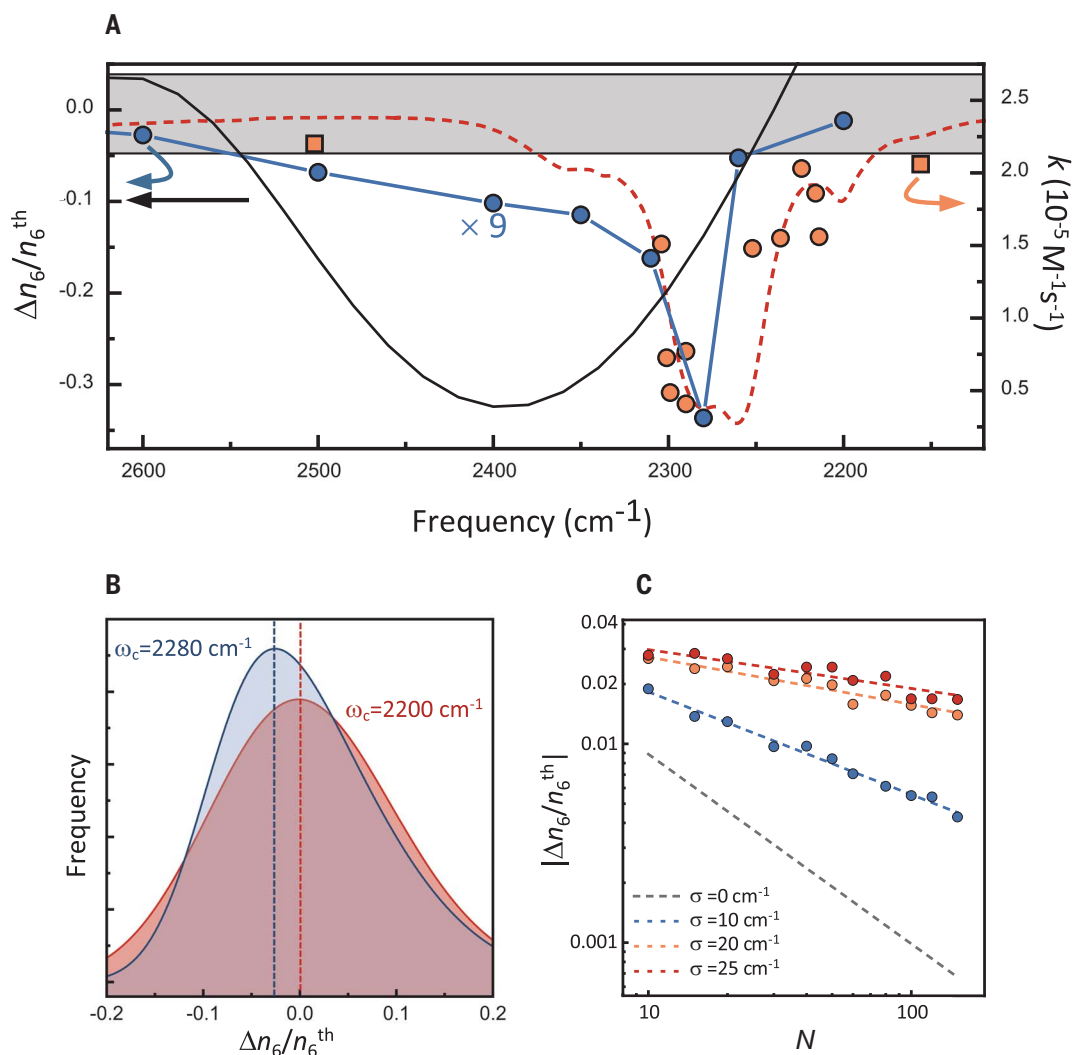
The action spectrum presented in (A) shows the extracted reaction rate constants (orange symbols) as a function of cavity tuning (i.e., Fabry-Perot mode position at normal incidence). The gray horizontal band represents the average out-of-cavity control rate with its width equal to the standard deviation of six measurements. Blue and orange dashed curves correspond, respectively, to initial and final transmission spectra. Reaction suppression was observed when the cavity was tuned to prominent vibrational modes. Several example linear fits, from which reaction rate constants were extracted, are shown in (B).

from canonical Boltzmann statistics. This phenomenon has been shown to occur for other strongly coupled subsystems (38), but its potential consequences in cavity chemistry have yet to be fully explored. In this picture, chemical bonds can break and form through local two-body processes with the vibrational level statistics modified by the strongly interacting photonic environment. This insight can be complemented by other approaches wherein the cavity photon quadrature is treated as another classical coordinate that contributes to a static polaritonic potential energy surface (39, 40).

In Fig. 3A, we show the deviation of the most-probable ν_6 occupation from its cavity-free canonical Boltzmann value, $\Delta n_6/n_6^{\text{th}}$, as a function of cavity frequency, for an ensemble of PHI molecules ($N = 50$) with a Gaussian distribution of ν_6 mode frequencies (variance = σ^2), coupled to a single cavity mode. Cavity-modified rate measurements (orange points reproduced from Fig. 2A) and the PHI transmission spectrum (orange dashed curve) are also shown. This single-mode theory predicted a narrow vibrational depopulation feature (blue

Fig. 3. Comparison of cavity-modified reactivity with theoretical prediction.

(A) The NCO region of the action spectrum of Fig. 2 is reproduced here. Single-mode theory predicted a resonant depopulation of the v_6 mode (blue points) that qualitatively followed the experimental data well. Example cavity-induced population redistribution is shown in (B). A multimode single-molecule treatment, solid black curve in (A), yielded a resonant depopulation effect that was considerably stronger in magnitude (note the $9\times$ scaling applied to the single-mode analysis) but was broader and blue-shifted relative to the experimental results. Although the cavity-induced effect was predicted to diminish with increased oscillator number, N , the scaling power strongly depended on molecular disorder (C). Molecular disorder, σ , was defined as a Gaussian broadening of the Lorentzian linewidth.



circles, $\Delta n_6/n_6^{\text{th}} < 0$) which closely followed the transmission lineshape and was most prominent at the frequency of the combination band (2280 cm^{-1}), in qualitative agreement with the measured action spectrum. Figure 3B shows that at large detuning, the vibrational occupation of v_6 was symmetrically centered at the canonical Boltzmann average, but near-resonant cavities gave a skewed distribution of $\Delta n_6/n_6^{\text{th}}$, whose most-probable value corresponded to net vibrational depopulation (additional histograms in fig. S14). The formal connection between $\Delta n_6/n_6^{\text{th}}$ and the reaction rate has yet to be developed (see ansatz in section 6 in the SM).

The single-mode many-particle analysis qualitatively agreed with the experimental data and improved our understanding of cavity-suppressed reactivity. However, the predicted values of $\Delta n_6/n_6^{\text{th}}$ were relatively small. This result was due to the many-particle model not accounting for the full dispersion of the cavity field. Treating large N and a continuum of cavity modes is prohibitive, but we could gain insight

by treating a single PHI molecule in a multimode Fabry-Perot cavity with a quasi-continuous spectrum ω_k , where k denotes the in-plane wave number (details in section 6.2 of the SM). We showed that $\Delta n_6/n_6^{\text{th}}$ in this case is proportional to $\sum_k (g_{6,k}/\gamma_6) \text{Im} \langle \hat{a}_k \hat{b}_6^\dagger \rangle_{\text{ss}}$, where $\langle \hat{a}_k \hat{b}_6^\dagger \rangle_{\text{ss}}$ is the stationary light-matter coherence between the vibrational mode and the k th cavity mode, $g_{6,k}$ is the Rabi frequency, and γ_6 is the homogeneous vibrational linewidth. Solving for the steady-state coherence gave

$$\Delta n_6/n_6^{\text{th}} = \sum_k P(\omega_k) \left(e^{-\Delta_{k,6}/k_B T} - 1 \right) \quad (1)$$

where $\Delta_{k,6} = \omega_k - \omega_{v_6}$ is the detuning of v_6 from the k th mode, and $P(\omega_k)$ is a normalized distribution function scaling with $(g_{6,k}/\Delta_{k,6})^2$ for $|\Delta_{k,6}| \gg \gamma_6$. Figure 3A (solid black curve) shows that the frequency response from Eq. 1 was much broader and blue-shifted relative to experiments. However, integrating over the cavity dispersion gave values of $\Delta n_6/n_6^{\text{th}}$ considerably

larger than the single cavity mode approach, suggesting that the entire photon spectrum contributed to cavity chemistry phenomena.

Finally, we addressed the N -scaling of the vibrational depopulation effect. Because the total vibration-cavity system was in thermal equilibrium (37), deviation of the photonic occupation from a canonical distribution by δn would correspond to a redistribution of vibrational occupation per molecule of $-\delta n/N$. Therefore, for typical values of $N \sim 10^6$ in Fabry-Perot cavities, the population redistribution on individual molecules should be negligible. However, in Fig. 3C we showed that this many-body dilution behavior did not hold in general for ensembles with frequency disorder, by plotting $\Delta n_6/n_6^{\text{th}}$ as a function of N for different values of the disorder width σ (see also fig. S15). We found that inhomogeneous broadening could protect resonant population redistribution from the homogeneous $1/N$ scaling, possibly due to partial delocalization of molecular states (41, 42).

Conclusions

In this work, we suppressed a ground-state addition reaction through strong coupling between molecular vibrational modes and cavity vacuum fields. This suppression reached 80%, and we found a strong cavity frequency dependence that closely followed the reactant infrared absorption spectrum. The strongest effect was for cavities resonant with an NCO mode that participated in the transition state of the reaction. We described the mechanism quantum mechanically as the emergence of stationary noncanonical vibrational populations as a result of strong vibration–cavity coupling but noted that the composite vibration–cavity polaritonic state remained in a Boltzmann thermal state. Deviations of the vibrational occupations from canonical statistics were due to stationary light–matter coherences that depended on the details of the cavity spectrum and dispersion. For molecular ensembles, we showed evidence that inhomogeneous spectral broadening could protect the light–matter coherences that influenced vibrational reactivity, suggesting fundamental links between chemistry and quantum science that have yet to be fully developed.

REFERENCES AND NOTES

- A. H. Zewail, *Phys. Today* **33**, 27–33 (1980).
- W. S. Warren, H. Rabitz, M. Dahleh, *Science* **259**, 1581–1589 (1993).
- T. Stensitzki *et al.*, *Nat. Chem.* **10**, 126–131 (2018).
- M. Delor *et al.*, *Science* **346**, 1492–1495 (2014).
- Z. Lin *et al.*, *J. Am. Chem. Soc.* **131**, 18060–18062 (2009).
- A. Assion *et al.*, *Science* **282**, 919–922 (1998).
- M. P. A. Branderhorst *et al.*, *Science* **320**, 638–643 (2008).
- A. Thomas *et al.*, *Angew. Chem. Int. Ed.* **55**, 11462–11466 (2016).
- A. Thomas *et al.*, *Science* **363**, 615–619 (2019).
- F. J. Garcia-Vidal, C. Ciuti, T. W. Ebbesen, *Science* **373**, eabd0336 (2021).
- B. S. Simpkins, A. D. Dunkelberger, J. C. Owrutsky, *J. Phys. Chem. C* **125**, 19081–19087 (2021).
- F. Herrera, J. Owrutsky, *J. Chem. Phys.* **152**, 100902 (2020).
- G. Khitrova, H. M. Gibbs, M. Kira, S. W. Koch, A. Scherer, *Nat. Phys.* **2**, 81–90 (2006).
- J. P. Long, B. S. Simpkins, *ACS Photonics* **2**, 130–136 (2015).
- A. Shalabney *et al.*, *Nat. Commun.* **6**, 5981 (2015).
- J. Del Pino, J. Feist, F. J. Garcia-Vidal, *New J. Phys.* **17**, 053040 (2015).
- J. A. Hutchison, T. Schwartz, C. Genet, E. Devaux, T. W. Ebbesen, *Angew. Chem. Int. Ed.* **51**, 1592–1596 (2012).
- B. Munkhbat, M. Wersäll, D. G. Baranov, T. J. Antosiewicz, T. Shegai, *Sci. Adv.* **4**, eaas9552 (2018).
- J. Lather, P. Bhatt, A. Thomas, T. W. Ebbesen, J. George, *Angew. Chem. Int. Ed.* **58**, 10635–10638 (2019).
- B. S. Simpkins *et al.*, *ACS Photonics* **2**, 1460–1467 (2015).
- C. Weisbuch, M. Nishioka, A. Ishikawa, Y. Arakawa, *Phys. Rev. Lett.* **69**, 3314–3317 (1992).
- W. Ahn, I. Vurgaftman, A. D. Dunkelberger, J. C. Owrutsky, B. S. Simpkins, *ACS Photonics* **5**, 158–166 (2018).
- S. Wang *et al.*, *J. Phys. Chem. Lett.* **5**, 1433–1439 (2014).
- A. D. Dunkelberger *et al.*, *ACS Photonics* **6**, 2719–2725 (2019).
- R. Houdré *et al.*, *Phys. Rev. B* **52**, 7810–7813 (1995).
- J. J. Pietron, K. P. Fears, J. C. Owrutsky, B. S. Simpkins, *ACS Photonics* **7**, 165–173 (2020).
- W. Ahn, B. S. Simpkins, *APL Photonics* **5**, 076107 (2020).
- M. V. Imperatore, J. B. Asbury, N. C. Giebink, *J. Chem. Phys.* **154**, 191103 (2021).
- G. D. Wiesehan, W. Xiong, *J. Chem. Phys.* **155**, 241103 (2021).
- E. Delebecq, J.-P. Pascault, B. Boutevin, F. Ganachaud, *Chem. Rev.* **113**, 80–118 (2013).
- F. Kössl, M. Lisaj, V. Kozich, K. Heyne, O. Kühn, *Chem. Phys. Lett.* **621**, 41–45 (2015).
- G. Raspoet, M. T. Nguyen, M. McGarraghy, A. F. Hegarty, *J. Org. Chem.* **63**, 6878–6885 (1998).
- A. A. Caraculacu, S. Coseri, *Prog. Polym. Sci.* **26**, 799–851 (2001).
- M. Çoban, F. A. S. Konuklar, *Comput. Theor. Chem.* **963**, 168–175 (2011).
- K. J. Laidler, *Chemical Kinetics* (Pearson Education Inc., 1987).
- C. Schäfer, M. Ruggenthaler, A. Rubio, *Phys. Rev. A* **98**, 043801 (2018).
- M. Seidel *et al.*, *ACS Photonics* **6**, 1823–1825 (2019).
- D. Xu, J. Cao, *Front. Phys. (Beijing)* **11**, 110308 (2016).
- T. E. Li, J. E. Subotnik, A. Nitzan, *Proc. Natl. Acad. Sci. U.S.A.* **117**, 18324–18331 (2020).
- C. Schäfer, J. Flick, E. Ronca, P. Narang, A. Rubio, *Nat. Commun.* **13**, 7817 (2022).
- D. Wellnitz, G. Pupillo, J. Schachenmayer, *Commun. Phys.* **5**, 120 (2022).
- M. Du, J. Yuen-Zhou, *Phys. Rev. Lett.* **128**, 096001 (2022).
- J. F. Triana, F. Recabal, F. Herrera, B. S. Simpkins, W. Ahn, Data: Modification of ground state chemical reactivity via light-matter coherence in infrared cavities, version 2, Zenodo (2023); <https://doi.org/10.5281/zenodo.7915873>.

ACKNOWLEDGMENTS

We thank J. Owrutsky, A. Dunkelberger, I. Vurgaftman, and J. Schachenmayer for discussions. **Funding:** This work was supported by US Naval Research Laboratory Nanoscience Institute, grant WU 1J03 (W.A. and B.S.S.); ANID Fondecyt Regular grant 1221420 (F.H.); ANID Fondecyt Doctorado grant 21221970 (F.R.); ANID Fondecyt Iniciación grant 11230679 (J.T.); Millennium Science Initiative Program grant ICN17_012 (F.H. and J.T.); and Programa de Cooperación Científica ECOS-ANID ECOS grant 200028 (F.H.). **Author contributions:** Conceptualization: B.S.S. and F.H. Methodology: B.S.S., F.H., and W.A. Investigation: W.A., J.F.T., F.R., F.H., and B.S.S. Visualization: B.S.S., J.F.T., and F.R. Funding acquisition: B.S.S. and F.H. Writing – original draft: W.A. and B.S.S. Writing – review & editing: B.S.S. and F.H. **Competing interests:** None declared. **Data and materials availability:** All data needed to support the conclusions of the main text and supplementary materials have been uploaded to Zenodo (43). **License information:** Copyright © 2023 the authors, some rights reserved; exclusive licensee American Association for the Advancement of Science. No claim to original US government works. <https://www.science.org/about/science-licenses-journal-article-reuse>

SUPPLEMENTARY MATERIALS

science.org/doi/10.1126/science.ade7147
Materials and Methods
Supplementary Text
Figs. S1 to S19
Tables S1 to S4
References (44–77)

Submitted 2 September 2022; resubmitted 7 March 2023
Accepted 12 May 2023
10.1126/science.ade7147



Modification of ground-state chemical reactivity via light–matter coherence in infrared cavities

Wonmi Ahn, Johan F. Triana, Felipe Recabal, Felipe Herrera, and Blake S. Simpkins

Science, **380** (6650), .

DOI: 10.1126/science.ade7147

Editor's summary

Hybrid light-matter states called polaritons, which are formed by strong interactions between resonant molecular transitions and photonic modes in microcavities, could be used to control chemical reactions with electromagnetic fields, a long-standing goal in chemistry. Unfortunately, such “polariton chemistry” still lacks a series of convincing demonstrations. Ahn *et al.* performed a joint experimental and theoretical study of alcoholysis of phenyl isocyanate with cyclohexanol under various strong light-matter coupling conditions. Through a rigorous analysis of their theoretical and experimental results, the authors provide compelling arguments for how cavity-altered reactivity may arise. These results are needed in this emerging field because they provide an important corroboration of earlier observations that became controversial after several reports of failed attempts. —Yury Suleymanov

View the article online

<https://www.science.org/doi/10.1126/science.ade7147>

Permissions

<https://www.science.org/help/reprints-and-permissions>

Use of this article is subject to the [Terms of service](#)

Science (ISSN) is published by the American Association for the Advancement of Science. 1200 New York Avenue NW, Washington, DC 20005. The title *Science* is a registered trademark of AAAS.

Copyright © 2023 The Authors, some rights reserved; exclusive licensee American Association for the Advancement of Science. No claim to original U.S. Government Works